Synthesis and Linear Optical Properties of Nanoscopic Gold Particle Pair Structures

Marie L. Sandrock and Colby A. Foss, Jr.*

Department of Chemistry, Georgetown University, Washington, District of Columbia 20057

Received: June 28, 1999; In Final Form: September 16, 1999

Pair particle nanostructures were prepared in porous anodic aluminum oxide films via a modified template synthesis procedure. By varying the interparticle distance of centrosymmetric gold spherical particles (radius ca. 32 nm), the linear UV/visible polarization spectra of the gold particle/porous alumina film composites can be altered. The resulting spectra can be explained qualitatively in terms of particle electromagnetic interactions within an individual pore through simple quasistatic limit scattering models. Modified long wavelength approximation and discrete dipole approximation methods yield similar calculated spectra, and neither approach quantitatively describes the experimental spectra. Discrepancies are interpreted to arise in part from a distribution of interparticle spacings in the experimental system. Rod, rod–pair, and rod–sphere gold nanoparticle structures were also synthesized. Possible evidence for interaction between the two members of the rod–sphere structure is seen in the experimental spectra. The polarization spectra of the rod-containing systems are also only qualitatively described by quasistatic limit models.

Introduction

It is well known that nanoscopic metal particles can exhibit strong absorption and/or scattering bands in the visible spectrum. This effect allows for a wide variety of practical applications of nanoscopic metal systems in the fine arts,[1] surface-enhanced spectroscopy,[2,3] nonlinear optics,[4–6] and biochemistry.[7] Significantly, the size and shape of these particles can be tuned to produce the desired linear optical effect, such as a specific spectral band position (λ_{max}) or an optimized local field enhancement factor for surface-enhanced Raman scattering studies.

The preparation of nanoscopic metal particles of nonspherical geometry has attracted much attention in the past decade. Lithographic methods have been used to prepare uniform arrays of ellipsoids[8] and truncated tetrahedra.[9] The template synthesis methods developed by Moskovits[10,11] and Martin[12,13] rely on the pore geometry of porous host materials to direct particle growth. Bulk solution synthesis of rodlike metal particles has been accomplished using surfactants that form cylindrical micelle superstructures in solution.[14] All of these synthesis methods have yielded nanoscopic metal particles whose UV/visible spectra are characteristic of nonspherical geometries. In the case of the porous template- or micelle-derived rods, the extinction spectra show long- and short-axis plasmon resonance bands which are the signature of such prolate structures.[6,12,14,15]

We recently extended the template synthesis method to prepare noncentrosymmetric nanoparticle structures involving two gold particles[6] and gold/silver iodide heterojunction particles.[16] In this paper, we describe how this modified template synthesis method can be used to prepare a variety of nanoparticle pair structures such as paired spheres, paired rods, and rod–sphere pairs. We discuss the plasmon resonance spectra of these different systems and, in the case of the paired-spheres, the spectral consequences of interparticle spacing. The experimental results are compared with spectra predicted from simple quasistatic theory and more advanced electrodynamic treatments.

Theoretical Considerations

The porous anodic alumina films employed as template hosts in this study are nonisotropic; they contain parallel arrays of pores which run normal to the face of the films. The optical spectra of the resulting gold nanoparticle–alumina composite materials thus depend strongly on the orientation of the film and the nanometal particle structures relative to the incident electric field. For nonnormal incidence under p-polarization (incident electric field polarized parallel to the plane of incidence), the plasmon resonance spectra of the present Au particle/alumina composites exhibit significant dependence on the incidence angle θ (the angle between the propagation vector and the sample surface normal); increasing θ typically leads to a red-shift in the plasmon resonance maximum or to the appearance of a second long-wavelength resonance. We review below the simple quasistatic limit treatments that describe, at least qualitatively, the spectral trends seen in experiment.

Single Particle Scattering Theory: Quasistatic Limit. The spectral properties of isolated nanoscopic particles can be understood on the basis of the well-known Clausius–Mossotti expression for particle polarizability:[17,18]

$$\alpha = \frac{4\pi\epsilon^o \mathbf{ab}^2}{3L_x}\frac{\epsilon_m - \epsilon_h}{\epsilon_m + \kappa\epsilon_h} \tag{1}$$

where ϵ_m and ϵ_h are the complex dielectric constants of the particle and host medium, respectively, and ϵ^o is the permittivity of vacuum. A rodlike structure can be reasonably approximated as an ellipsoid of revolution, with semimajor axis $\mathbf{a}$ and semiminor axis $\mathbf{b}$. The parameters L_x and κ are the depolarization and screening factors, respectively. They depend only on particle shape and orientation in the incident field and are related to each other via $\kappa = L_x^{-1} - 1$. The calculation of extinction cross-section C_{ext} from the particle polarizability is straightforward.[17,18]

Interacting Particle Pairs. Quasistatic limit expressions for two-particle and larger clusters have been described by Kreibig and Vollmer.[19] The derivation of the expression for an axisymmetric structure of two particles is simple and worthy of a brief

* Corresponding author e-mail fossc@gusun.georgetown.edu.

Nanoscopic Gold Particle Pair Structures

J. Phys. Chem. B, Vol. 103, No. 51, 1999 **11399**

summary here. The electric dipole moments of the two particles are given by

$$\mu_1 = \epsilon_h \alpha_1 \mathbf{E}_1 \tag{2a}$$

$$\mu_2 = \epsilon_h \alpha_2 \mathbf{E}_2 \tag{2b}$$

where $\mathbf{E}_1$ and $\mathbf{E}_2$ are the electric fields experienced by particles 1 and 2, respectively. The field at each particle may be assumed to be the sum of the applied field $\mathbf{E}$ in the material and a contribution arising from the other particle. For example, the fields at particles 1 and 2 can expressed as

$$\mathbf{E}_1 = \mathbf{E} + g\frac{\mu_2}{\epsilon_h \epsilon^o d_{12}^3} \tag{3a}$$

$$\mathbf{E}_2 = \mathbf{E} + g\frac{\mu_1}{\epsilon_h \epsilon^o d_{12}^3} \tag{3b}$$

where d_{12} is the center-to-center distance between the two particles and g is a geometric factor that depends on the orientation of the particle pair in the applied field. Substitution of eqs 2 into eqs 3, and subsequent combination of 3a and 3b leads to two expressions which describe the relationship between the applied field and the actual field at a given particle:

$$\mathbf{E}_1\left(1 - g^2\frac{\alpha_1\alpha_2}{d_{12}^6}\right) = \mathbf{E}\left(1 + g\frac{\alpha_2}{d_{12}^3}\right) \tag{4a}$$

$$\mathbf{E}_2\left(1 - g^2\frac{\alpha_1\alpha_2}{d_{12}^6}\right) = \mathbf{E}\left(1 + g\frac{\alpha_1}{d_{12}^3}\right) \tag{4b}$$

The average polarizability $\langle\alpha\rangle$ of the particle pair is defined according to the relations

$$\frac{1}{2}(\mu_1 + \mu_2) = \epsilon_h\frac{1}{2}(\alpha_1\mathbf{E}_1 + \alpha_2\mathbf{E}_2) = \epsilon_h\langle\alpha\rangle\mathbf{E} \tag{5}$$

Combining eqs 4 and 5 leads to

$$\langle\alpha\rangle = \frac{1}{2}\frac{\alpha_1\left(1 + g\frac{\alpha_2}{d_{12}^3}\right) + \alpha_2\left(1 + g\frac{\alpha_1}{d_{12}^3}\right)}{\left(1 - g^2\frac{\alpha_1\alpha_2}{d_{12}^6}\right)} \tag{6}$$

To obtain the extinction spectrum for the particle pair structure, the average polarizability is inserted into the standard C_{ext} expressions. For the case of an electric field incident along the particle pair axis (longitudinal polarization), the geometric factor g is equal to $1/2\pi$. For an electric field incident perpendicular to the axis of rotation (transverse polarization), $g = -1/4\pi$.[20] For intermediate incidence angles θ, the average extinction is the weighted sum of the longitudinal and transverse polarization cases:[18]

$$C_{ext}(\theta) = C_{ext,\parallel}\sin^2(\theta) + C_{ext,\perp}\cos^2(\theta) \tag{7}$$

Equation 7 pertains specifically to the case where the rotational axes of the particles are perpendicular to the surface planes of the thin film sample and the incident field is p-polarized (vide infra).

Experimental Section

Porous Aluminum Oxide Synthesis. Porous aluminum oxide films were prepared using the anodization/voltage reduction
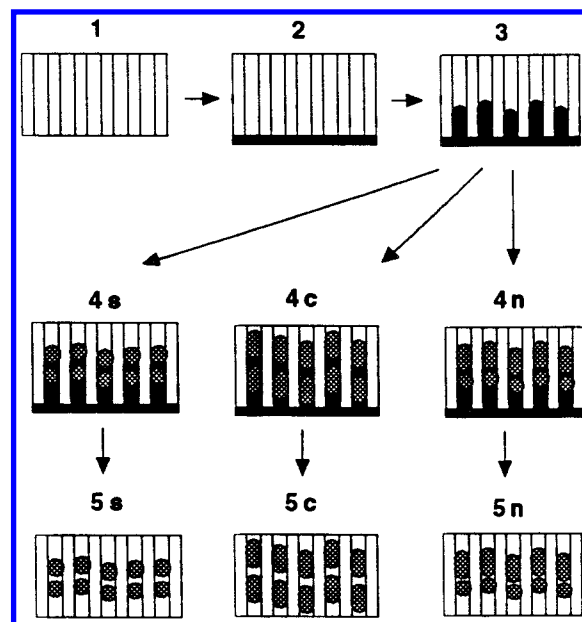

Figure 1. Schematic of gold nanoparticle pair synthesis. One face of the porous anodic alumina film (1) is sputtered with Ag (2). A silver foundation is electrochemically deposited (3). Additional layers of Au, Ag spacer, and Au again are electrochemically deposited onto the silver foundation (4). The Ag foundation and spacers are removed by nitric acid etching (5) to yield the Au pair structures. The letters s, c, and n refer to spheres, centrosymmetric, and noncentrosymmetric structures, respectively.

method of Furneax et al.[21] The details of our procedure have been given elsewhere.[13,15] In this study, we employed porous alumina films prepared via anodization of aluminum foil (Aldrich, 99.999%) at 20 V in 6% sulfuric acid at 0 °C. The mean pore diameters of these films were determined (via TEM analysis) to be 32 ± 1 nm. Typical film thicknesses were in the $40-60$ μm range.

Gold Nanoparticle Preparation. The porous alumina films were used as a template to synthesize gold rods, rod−pair structures, paired rod−sphere structures, and paired spheres with two different distances of separation. To create a conductive foundation upon which subsequent electrochemical deposition would occur, the barrier side of the porous alumina films were sputtered with ca. 45 nm of silver using an Anatech Hummer 10.2 plasma deposition device.

Electrochemical deposition of Ag and Au were done using a three-electrode cell equipped with an Ag/AgCl reference electrode, a platinum mesh counter electrode, and the Ag-sputtered porous alumina film as the working electrode (area 3.14 cm^2). A $0.80-1.27$ C/cm^2 foundation of silver was electrodeposited over the 3.14 cm^2 film area potentiostatically (-0.6 V vs Ag/AgCl) from a silver thiocyanate (Ag(I)) plating solution.[22] This foundation ensured that the subsequent Au deposition would occur at a depth in the film where the pore structure is well-defined. Au layers were deposited potentiostatically (-0.9V vs Ag/AgCl) from an Au(I) plating solution (Orotemp 24, Technic, Inc.).

The electrochemical template synthesis scheme for the paired spheres, paired rods and rod−sphere pairs is shown in Figure 1. For closely spaced paired sphere structures, the first Ag deposition was followed by deposition of 0.03 C/cm^2 of Au(I), 0.02C/cm^2 of Ag(I), and a second Au(I) deposition of 0.03 C/cm^2. The Ag foundation and spacer structures were then removed by soaking the films in nitric acid (EM Sciences, 69−71%) for twenty minutes. The films were then rinsed in deionized water, ethanol, and acetone, and then allowed to dry
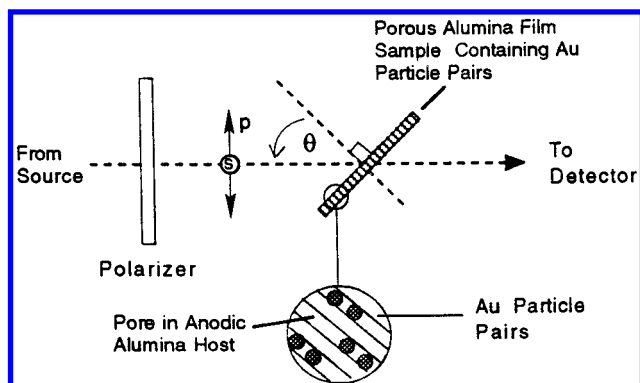
Figure 2. Schematic of polarization spectroscopy setup. The sample film is rotated about an axis perpendicular to the page. The angle of incidence is indicated by θ. p-Polarization corresponds to an incident electric field polarized in the plane of the page. s-Polarization corresponds to an electric field oscillating normal to the page.

at room temperature. The films were then placed in an oven for 30 min at 130 °C to anneal the Au layers to a spherical geometry. For the paired spheres with larger spacing, the procedure was the same except that 0.03 C/cm^2 of Ag(I) was deposited as the spacer layer.

The centrosymmetric paired rod structures were prepared in a similar fashion. After the initial Ag foundation was deposited, two layers of Au(I) were deposited (0.19 C/cm^2), separated by an Ag spacer layer formed via deposition of 0.03 C/cm^2 Ag(I). The rod−sphere structures were formed via deposition of 0.03 C/cm^2, 0.03 C/cm^2, and 0.16 C/cm^2 of Au(I), Ag(I), and Au(I), respectively. The Ag layers were removed via HNO$_3$ etching and rinsed in deionized water, ethanol, and acetone. Oven annealing was not performed on rod-containing composites.

Nanoparticle Characterization. Transmission electron microscopy (TEM) was used to characterize the dimensions of the template-synthesized gold nanostructures. The alumina films

containing the Au nanostructures were immersed in resin and microtomed (to ca. 70 nm thickness). The microtomed samples were then placed on 200 mesh Cu grids (EM Sciences) for examination in a JEOL 1200 EX microscope. Details of sample preparation and TEM analysis have been described elsewhere.[6]

Spectroscopic Analysis of the Nanoparticle Composites. Linear polarization analysis of the composite films was performed using a Hitachi U-3501 spectrophotometer equipped with a model 210-2130 polarizer accessory. Extinction spectra were obtained between $\lambda = 350$ nm and $\lambda = 800$ nm at normal incidence (defined as $\theta = 0°$ and corresponding to the case where the incident electric field is perpendicular to the pore axes) and at incidence angles $\theta = 20°$, 30°, and 45°, under p-polarization (the incident electric field polarized parallel to the plane of incidence). A schematic of the sample/polarizer configuration is shown in Figure 2.

Results and Discussion

Transmission Electron Microscopy. Figure 3 shows the TEM images of the paired-sphere structures in porous alumina. These images are cross-sectional. For the system in which 0.02 C/cm^2 Ag(I) were deposited to form a spacer layer, the average Au sphere diameter is 35 ± 4 nm. The surface-to-surface separation distance is 20 ± 10 nm. For the pair system in which 0.03 C/cm^2 Ag(I) was deposited as the spacer, the average spacing is 84 ± 6 nm. The average sphere diameter was found to be 30 ± 2 nm.[23]

Figure 4 depicts cross-sectional TEM images of both centrosymmetric and noncentrosymmetric pair structures and a single-Au rod composite prepared for spectroscopic comparison (Figure 4A). The single rod structures have an average length $a = 133 \pm 20$ nm and diameter $b = 31 \pm 4$ nm. The individual rods in the centrosymmetric rod−pair structures (Figure 4B) have an average length $a = 70 \pm 10$ nm and a diameter $b = 30 \pm 3$ nm. The interparticle spacing is 70 ± 20 nm. The
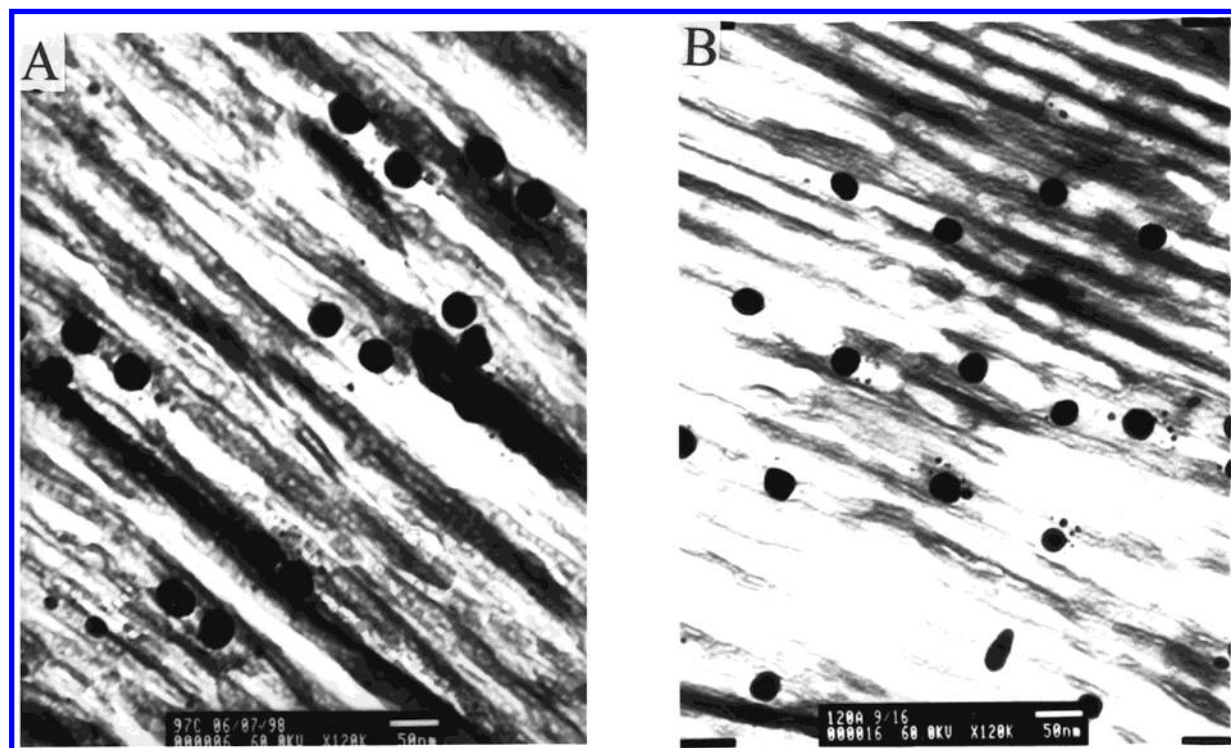

Figure 3. Transmission electron microscope images of 0.03 C/cm^2 Au centrosymmetric Au pair particles in an alumina host. (A) 16 nm radius Au particles with smaller interparticle spacing after deposition of 0.02 C/cm^2 Ag(I) spacer. (B) 16 nm radius Au particles with larger spacing after deposition of 0.03 C/cm^2 Ag(I) spacer. Scale bar in both cases corresponds to 50 nm.
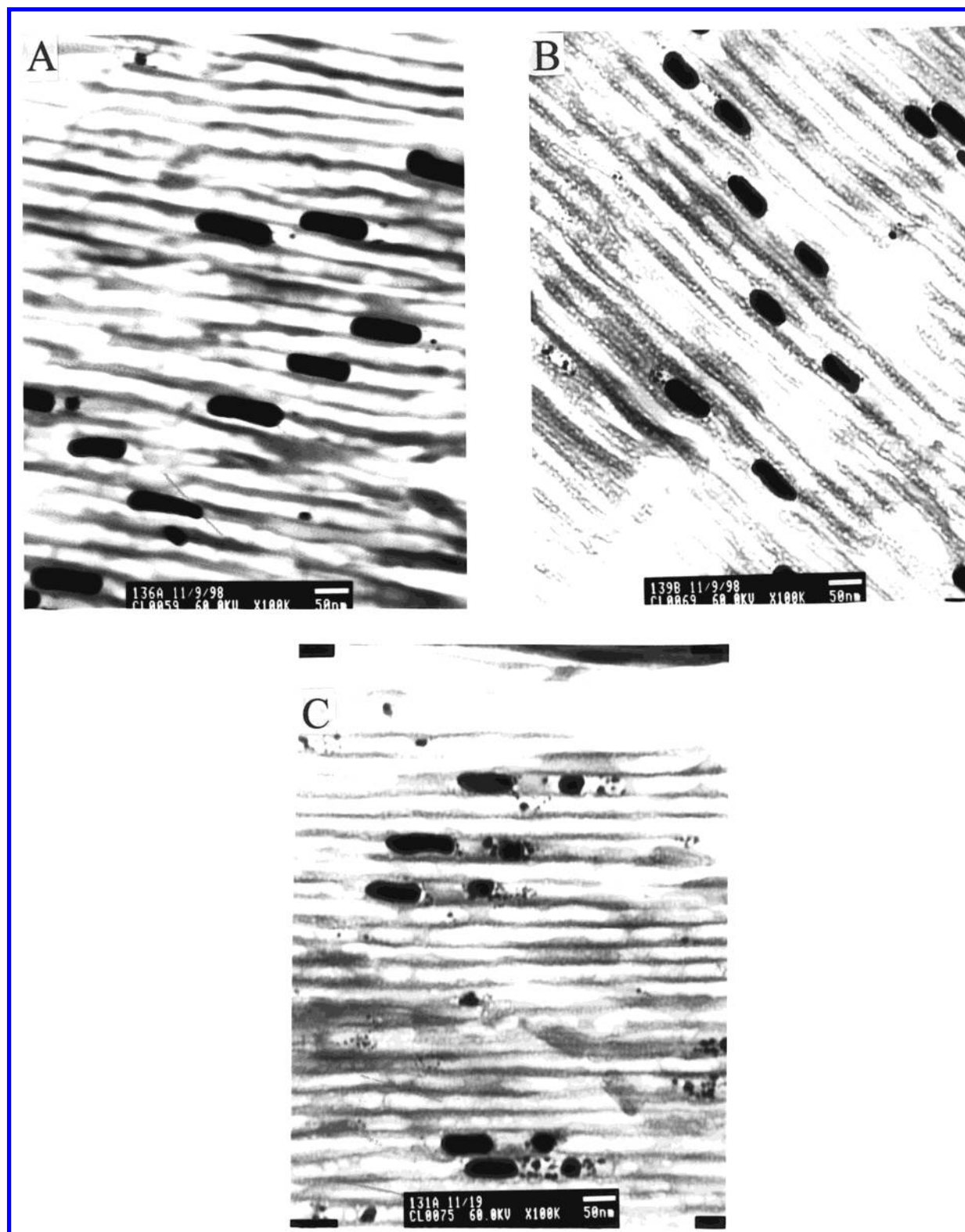
Figure 4. Transmission electron microscope images. (A) 0.19 C/cm² Au centrosymmetric particles in alumina host. (B) 0.19 C/cm² Au centrosymmetric pair particles in alumina (0.10 C/cm² Au(I) deposited for both segments). (C) 0.19 C/cm² Au noncentrosymmetric pair particles in alumina host (0.16 C/cm² Au(I) deposited for larger segment, 0.03 C/cm² Au(I) deposited for small segment). Scale bar in all cases corresponds to 50 nm.

noncentrosymmetric pair structures (Figure 4C) are composed of a rodlike segment ($a = 100 \pm 10$ nm, $b = 33 \pm 4$ nm) and a sphere-like segment ($a = 34 \pm 5$ nm, $b = 33 \pm 4$ nm). The separation distance between the rod and sphere segments is 57 $\pm$ 13 nm.

Effect of Interparticle Spacing in Paired-Sphere Structures. UV/vis polarization spectra of the Au/Al$_2$O$_3$ composite films were measured using the sample configuration shown in

Figure 2. The spectra were obtained at normal incidence and at incidence angles $\theta = 20°$, $30°$, and $45°$, with the electric field polarized in the plane of incidence (p-polarization). Figure 5 shows the spectra of the paired sphere structures whose TEM images are shown in Figure 3. For the Au pairs with large interparticle spacing (5A), the plasmon resonance maximum λ_{max} occurs at 548 nm for all incidence angles. For the pair structures with smaller separation distance (5B), λ_{max} occurs at ca. 539

11402 *J. Phys. Chem. B, Vol. 103, No. 51, 1999*
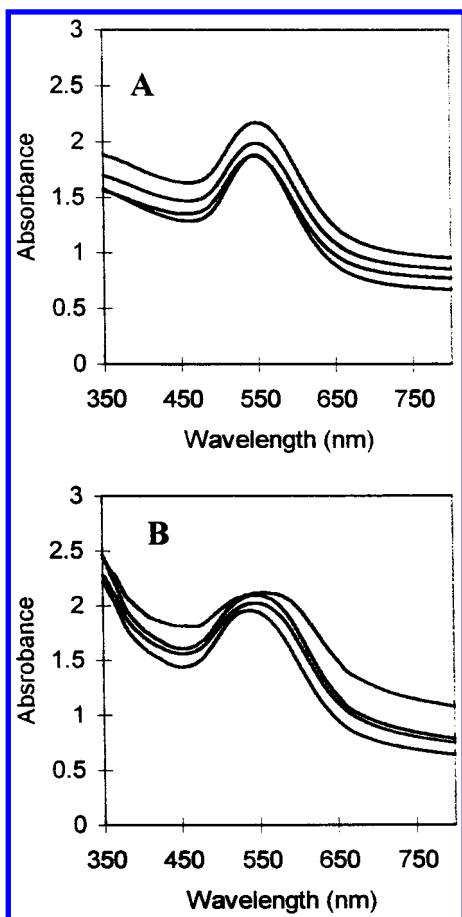
Sandrock and Foss

Figure 5. Plasmon resonance spectra of 16 nm radius Au sphere pair systems (p-polarization). (A) Large interparticle spacing (d_{12} ca. 114 nm). (B) Smaller interparticle spacing (d_{12} ca. 52 nm). In both figures, an increasing overall extinction corresponds to increasing incidence angle θ (0, 20, 30, and 45 degrees). All spectra were obtained in double-beam mode with no material in the reference beam.
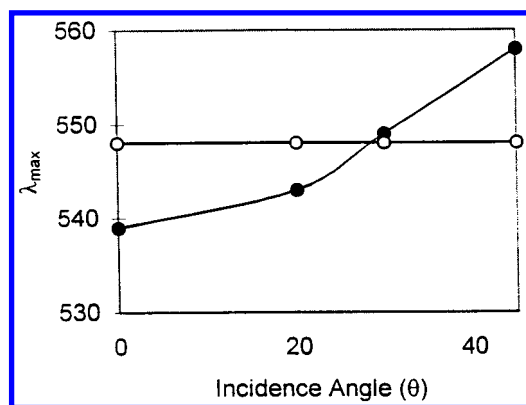

Figure 6. Experimental λ_{max} (nanometers) versus incidence angle θ (p-polarization) for Au sphere pair systems. Open circles: $d_{12} = 114$ nm. Closed circles: $d_{12} = 52$ nm.

nm at normal incidence and progressively red-shifts with increasing incidence angle. At $\theta = 45°$, $\lambda_{max} = 558$ nm. The width of the plasmon resonance band also increases with increasing θ. In both sets of spectra, the overall extinction intensity increases with increasing incidence angle. This observation is consistent with an increasing effective optical path length through the porous aluminum oxide. The λ_{max} trend with incidence angle for the two Au sphere-pair structures is shown in Figure 6. The Au sphere structures with an average separation distance of 20 nm show not only a significant dependence on

θ, but a λ_{max} at normal incidence that is lower than that of isolated 32 nm Au spheres in alumina.

We first compared the experimental spectra with those calculated for 32 nm Au sphere pairs using the quasistatic limit treatment for $\langle\alpha\rangle$ given by eq 6. Optical data for gold were taken from Johnson and Christy,[24] and the host oxide refractive index was assumed to be 1.33. When the interparticle spacing d_{12} is assumed to be 114 nm, the plasmon resonance band shows no dependence on the incidence angle. At 52 nm spacing, increasing θ results in a red-shifted plasmon resonance maximum, a result in qualitative accord with experiment. However, the absolute values for λ_{max} are underestimated relative to experiment at all incidence angles. Furthermore, for the 52 nm separation pair, total difference $\Delta\lambda_{max}$ ($= \lambda_{max}$ (45°) $- \lambda_{max}(0°)$) is ca. 20 nm in experiment but only ca. 6 nm in the spectra simulated using eq 6.

Calculations based on eq 6 assume that the Au particles are negligibly small relative to the incident wavelength. Of course, we have not achieved this condition in experiment. To address the finite size of the Au particles, we calculated polarization spectra for 32 nm Au spheres using the well-known modified long wavelength approximation (MLWA). The MLWA involves replacing the particle size independent depolarization factor L_x in eq 1 with the size-dependent quantity[25]

$$L_{x,\text{eff}} = L_x - \frac{1}{3} k^2 a^2 - \frac{2}{9} ik^3 a^3 \tag{8}$$

where k is the wave vector ($=2\pi\tilde{n}_h/\lambda$) and a is the sphere radius.

Figures 7A and B show extinction spectra calculated for the Au spheres separated by 84 and 20 nm gaps, which correspond to d_{12} values of ca. 114 and 52 nm, respectively.[26] At large separation (Figure 7A), the dependence of λ_{max} on θ is still negligible, though the λ_{max} values themselves are red-shifted slightly relative to the simple quasistatic result. For $d_{12} = 52$ nm, $\Delta\lambda_{max}$ is ca. 10 nm, compared to 6 nm in the quasistatic calculation. In the case of contacting Au spheres, the θ-dependence of the extinction intensity and $\Delta\lambda_{max}$ are both much more pronounced, with the latter quantity ca. 30 nm.

Another factor in the experiment, theory discrepancy is the distribution of interparticle separations. An average surface−surface separation of 20 ± 10 nm implies a significant fraction of pairs with smaller separation distances whose λ_{max} dependence on θ is stronger than that shown in Figure 7B. For example Figure 7C shows polarization spectra calculated for the extreme case of 32 nm Au spheres in contact ($d_{12} = 32$ nm). The net change in the extinction maximum $\Delta\lambda_{max}$ is 24 nm, a number comparable to experiment. Conversely, the population fraction that involves larger separations will show a weaker dependence of λ_{max} on θ. We find that the calculated extinction cross section increases with decreasing interparticle separation. This implies that the measured spectrum, which is the sum of the extinction of all particle pairs, may tend to be dominated by the more closely spaced particles. Indeed, the experimental plasmon resonance bands broaden and become asymmetric as the incidence angle increases, an observation consistent with a distribution of interparticle separations.

Introducing particle size corrections into the simple quasistatic theory yields only a slight improvement in the theory−experiment comparison. Indeed, regardless of particle size corrections, eq 6 assumes that neighboring particles can be treated as point dipole field sources and necessarily avoids the details of surface charge distribution. Furthermore, only dipole induction modes are considered; quadrupole and higher multipole modes are ignored. Finally, the finite size and center-to-
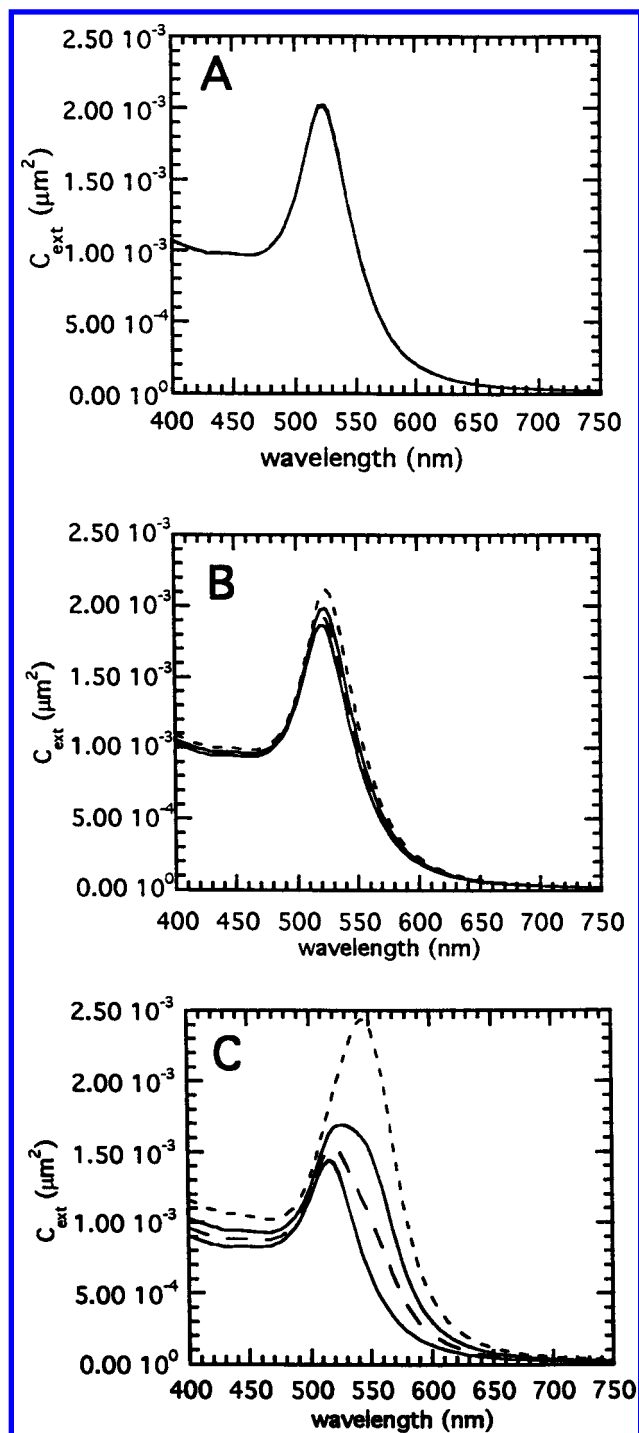
Nanoscopic Gold Particle Pair Structures

J. Phys. Chem. B, Vol. 103, No. 51, 1999 **11403**

Figure 7. Plasmon resonance spectra of 16 nm radius gold sphere pairs calculated for various incidence angles under p-polarization using MLWA model. (A) $d_{12} = 114$ nm. (B) $d_{12} = 52$ nm. (C) $d_{12} = 32$ nm (spheres touching). Increasing overall extinction corresponds to the incidence angle θ progression: 0, 20, 30, and 45 degrees.

center separation distances between two nanoscale particles results in their experiencing different phases of the incident oscillating field.[19,27] This issue is also ignored in models based on eq 6.

A more rigorous treatment of the extinction spectrum of interacting particle pairs and other complex structures is clearly needed and is fortunately available in the so-called discrete dipole approximation (DDA).[28,29] The DDA treats each particle as a cubic array of polarizable elements, each element capable of producing only a dipolar response to the applied field. However, the extinction spectrum of a particle treated as a large

collection of dipole elements exhibits features that correspond to quadrupole and higher multipole induction modes. A thorough evaluation of the DDA applied to nanoscopic metal particles, including comparisons with Mie theory and the MLWA, is given by Jensen et al.[30]

We have applied the DDA to 32 nm gold particle pairs at 114, 54, and 32 nm center-to-center separations. The host medium real refractive index was assumed to be 1.33. The number of polarizable elements assumed for each particles was large (1791 to 14 398), the optimal number depending on the interparticle spacing.[31] Extinction spectra were calculated for the limiting cases where the incident electric field was polarized parallel and perpendicular to the pair axis. Spectra corresponding to incidence angles $\theta = 0°$, 20°, 30°, and 45° were then produced using eq 7. The results of the DDA calculations are shown in Figure 8. They are surprisingly similar to the MLWA results in terms of peak position and intensity trends. In the case of the spheres in contact, the DDA spectra show an increase in extinction at long wavelengths, a feature not seen in the quasistatic and MLWA results. This long wavelength feature in the DDA result may be due to a second Au particle resonance in the near-infrared spectrum. Calculations by Jensen et al. show two major resonance bands for contacting 30 nm silver spheres in a vacuum, one near 400 nm and another near 800 nm. The behavior of two contacting gold spheres should be similar but with both resonances at longer wavelengths. We should note, however, that we do not see evidence of a second resonance in our experimental UV/vis spectra.

For gold spheres in close proximity, all of the theoretical treatments considered predict a spectroscopic red-shift in λ_{max} with increasing incidence angle θ. While this result is in qualitative accord with experiment, the ubiquitous prediction of a large increase in extinction intensity accompanying the red-shift is not seen in the experimental data. It should be noted that all of the spectral simulations are based on so-called single-particle scattering models; extinction is assumed to arise solely from the gold particle structures and not from absorption and/or reflection losses due to the host material. In the experimental systems, the net effect of reflection and absorption losses from the alumina host is an increasing vertical displacement of the plasmon resonance bands with increasing incidence angle. Since the spectrum of anodic aluminum oxide is featureless between ca. 400 and 800 nm,[13] this displacement is roughly constant over the visible spectral range and cannot act to selectively diminish the long-axis plasmon resonance bands (or selectively enhance the short-axis bands).

Polarization Spectra of Rods, Rod Pairs and Rod-Sphere Pairs. Figure 9 shows the UV/vis spectra of various Au particle/alumina composites at four incidence angles under p-polarization. While the absolute amount of gold deposited in the three composites is similar, the manner in which the metal is distributed in the composite has a direct effect on the plasmon resonance spectra. Figure 9A shows the polarization spectra for the composite in which the gold is deposited in a single step to yield long rods. At normal incidence, a single band centered at 516 nm corresponding to the rod's short-axis polarization is observed. As the incidence angle θ is increased, a second band corresponding to the long-axis resonance appears, the λ_{max} of which is centered in the near-infrared spectrum and out of the working range of the film polarizer.

Subdividing the gold deposit into two 70 nm long segments separated by a 70 nm gap leads to the spectra shown in Figure 9B. At normal incidence the spectrum shows a single band centered at ca. 517 nm. As θ is increased, the long-axis

11404 *J. Phys. Chem. B, Vol. 103, No. 51, 1999*
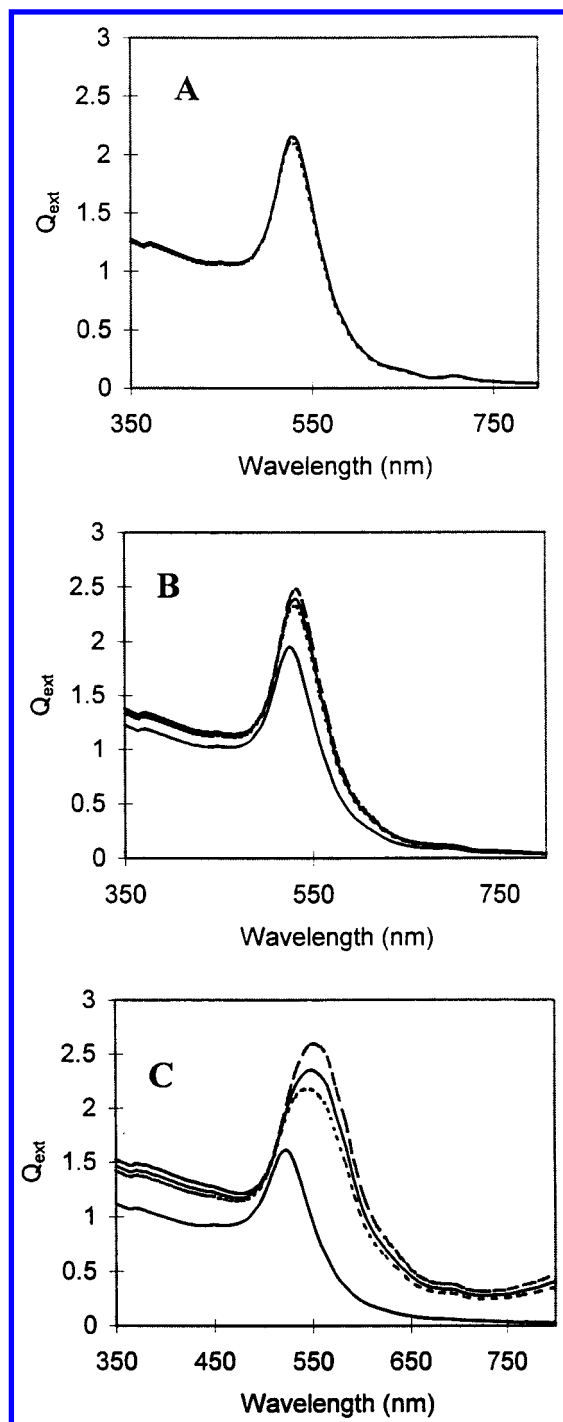
Sandrock and Foss

Figure 8. Plasmon resonance spectra of 16 nm radius gold sphere pairs calculated using the DDA model. Interparticle spacings for A, B and C as given in Figure 7. The number of polarizable elements assumed for each sphere are: A: 1791; B: 4224; C: 14398. Note that $Q_{ext} = C_{ext}/\pi a^2$.

Figure 9. UV/visible p-polarization spectra at incidence angles 0, 20, 30, and 45 degrees. (A) Centrosymmetric Au particle/alumina composite. (B) Centrosymmetric Au pair particle/alumina composite. (C) Noncentrosymmetric pair particle/alumina composite. Incidence angles are indicated next to curves.

resonance centered at 660 nm appears. The λ_{max} values for the long-axis plasmon resonance band is close to that observed for gold rods of similar dimensions (but not present as pairs) embedded and oriented in polyethylene.[15] This suggests that the 70 nm gap is large enough to preclude strong interparticle interactions and that the two segments behave essentially as independent rods.

Figure 9C shows the polarization spectra of the Au/alumina composites in which the deposited gold is distributed into asymmetric rod–sphere structures. At normal incidence, the single plasmon resonance band maximum occurs at a longer
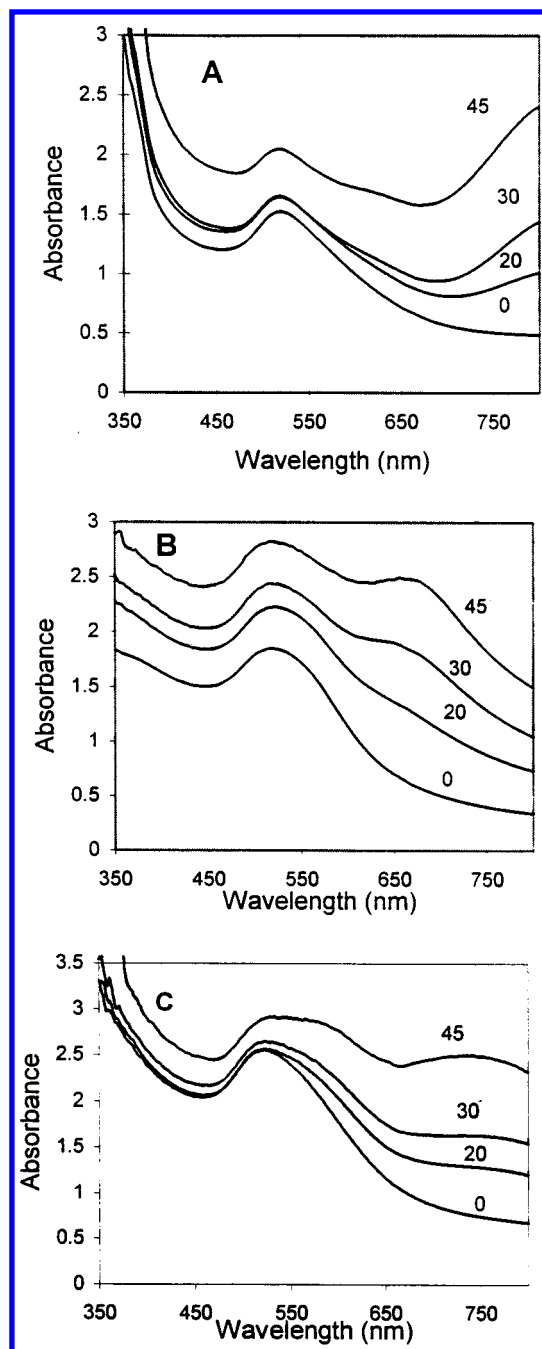
wavelength than in the cases of the other two rod-containing composites. We interpret this as resulting from a large extinction contribution from the sphere member of the pair. As the incidence angle is increased, a long axis resonance appears, centered at about 725 nm. While the general trends with θ are similar to the other rod-containing composites, the rod–sphere pair system shows an additional feature. As the incidence angle increases, a shoulder band develops on the long-wavelength slope of the resonance centered at 520 nm.

The polarization spectra of the gold rod, rod–pair, and rod–sphere pair composites can be explained qualitatively on the basis of the quasistatic theory outlined earlier. At normal incidence, the electric field is directed exclusively across the short axis of the gold rods. In this orientation, the screening
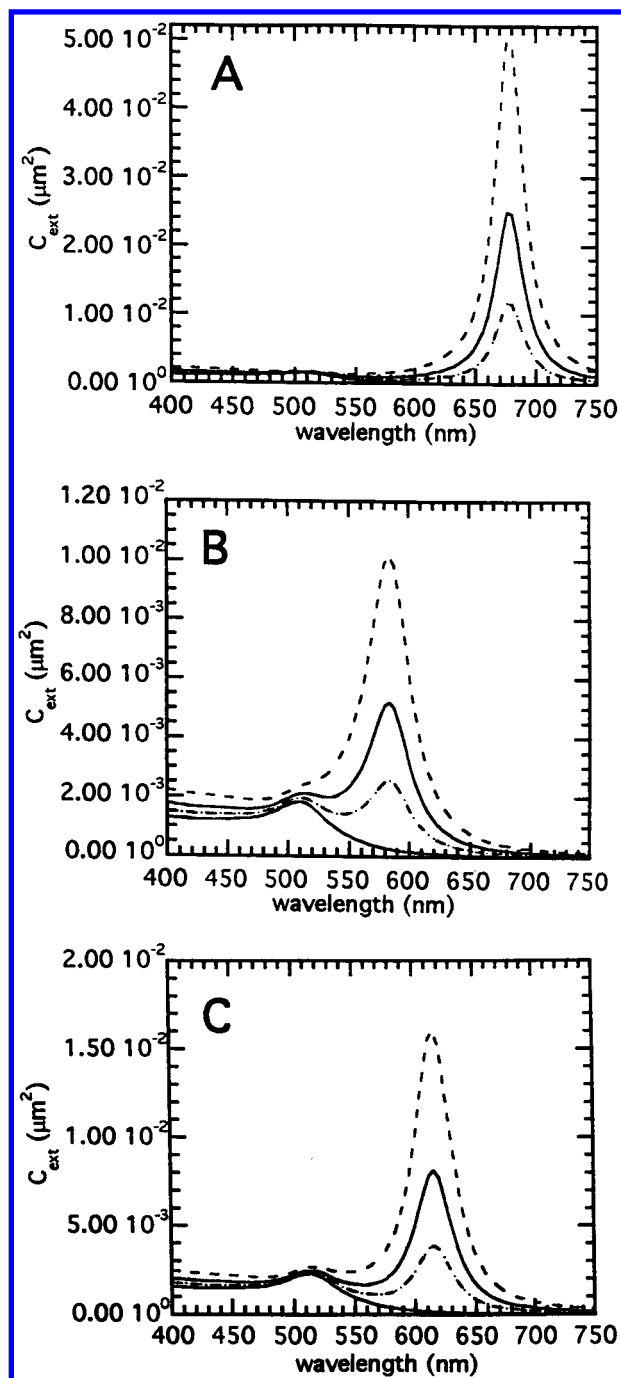
Figure 10. Quasistatic limit model spectra for rod-containing composites under p-polarization at incidence angles 0, 20, 30, and 45 degrees. (A) Rods. (B) Rod pairs ($d_{12} = 70$ nm). C. Rod−sphere pairs ($d_{12} = 57$ nm). Increasing overall extinction corresponds to increasing incidence angle θ.

parameter κ is less than 2. The screening parameter κ for **E** parallel to the long axis is larger than that corresponding to the short axis, and thus the plasmon resonance condition (the wavelength at which $\epsilon_m = -\kappa\epsilon_h$) occurs at a longer wavelength. As the incidence angle increases under p-polarization, the component of the electric field along the long axis of the particles also increases, and the long wavelength band becomes more pronounced.

Figure 10 shows the polarization spectra calculated using eq 6 and the average dimensions and spacings of the three gold particle/alumina composites obtained from TEM images. The qualitative trend in band position is the same as seen in experiment. However, in all cases, the relative intensity of the

long-axis resonance band is much higher than in experiment, and the theoretical λ_{max} values are less than those seen in Figure 9. A similar discrepancy was noted in our earlier work on oriented gold rods in polyethylene.[15] The large apparent short-axis extinction intensity may arise from spherical Au impurity particles, as seen in solution-phase surfactant-based syntheses.[14] However, we do not observe a significant number of spherical particles in the TEM images (except those which have been intentionally synthesized). Also, in the Au rod/polyethylene study, which employed an identical template synthesis procedure, the polarization spectra did not indicate a large number of spherical Au particles.[32]

One interpretation of the shoulder feature seen in the rod−sphere composite (Figure 9C) is that it arises from a red-shift of the sphere resonance due to interactions with the nearby rod. Since this feature is not reproduced in the quasistatic model spectra (Figure 10C), an alternate interpretation is that it is a quadrupole mode of the rod component. We should note, however, that based on previous T-matrix scattering simulations and experimental data for large aspect ratio gold rods (16 nm radius) such modes are expected to be weak, at least for isolated particles.[15] Simulations based on the MLWA grossly overestimated the λ_{max} values for both the long- and short-axis resonances of the rod pair and rod−sphere systems. DDA calculations on these structures are in progress.

Conclusions

Porous alumina based template synthesis can be used to prepare paired metal nanoparticle structures. The average spacing between the members can also be controlled, though the distribution of spacings is large. In the case of the sphere pairs, the interparticle spacing has an observable effect on the measured spectra. When the average surface-to-surface distance is about three particle diameters, an increase in incidence angle has no effect on the plasmon resonance peak position. At the smaller interparticle spacing (corresponding to less than one particle diameter), an increase in incidence angle causes a red-shift and broadening of the resonance band.

Rod pair and rod−sphere pair structures can also be achieved with the template method. The particular structures prepared in this study show polarization spectra generally similar to those observed for gold rods oriented in polyethylene. The interparticle spacing in the rod pair system is apparently large enough to allow each rod to respond independently to the applied field. The spectra corresponding to the rod−sphere pair system may indicate some electromagnetic interaction between the members.

The experimental spectra of the sphere pair systems were compared with simulations based on simple quasistatic, MLWA, and DDA models. For the sphere pair dimensions considered here, the MLWA and DDA calculations yield similar results. While incidence angle dependent trends were reproduced in all three models, none of these approaches yielded quantitative agreement with experiment, either in terms of peak position or shape. Discrepancies in peak shape may arise in part from the distribution of interparticle spacings.

Quasistatic limit simulations of the spectra of the rod-containing composites also agreed only qualitatively with experiment. The relative intensities of the long axis extinctions were always larger in theory than in experiment. Subtle spectral features observed in the rod−sphere pair experimental spectra could not be reproduced with quasistatic model.

References and Notes

(1) Lam, D. M. K.; Rossiter, B. W. *Sci. Am.* **1991**, *November*, 80.

(2) Chumanov, G.; Sokolov, K.; Gregory, B. W.; Cotton, T. M. *J. Phys. Chem.* **1995**, *99*, 9466.

(3) Moskovits, M. *Rev. Mod. Phys.* **1985**, *57*, 783.

(4) Hache, F.; Klein, R. D.; Flytzanis, C. *J. Opt. Soc. Am. B* **1986**, *3*, 1647.

(5) Flytzanis C.; Hache, F.; Klein, M. C.; Richard, D.; Roussingnol, P. In *Progress in Optics*; Wolf, E., Ed., North-Holland: Amsterdam, 1991, *29*, 323.

(6) Sandrock, M. L.; Pibel, C. D.; Geiger, F. M.; Foss, C. A., Jr. *J. Phys. Chem. B.* **1999**, *103*, 2668.

(7) Storhoff, J. J.; Elghanian, R.; Mucic, R. C.; Mirkin, C. A.; Letsinger, R. L. *J. Am. Chem. Soc.* **1998**, *120*, 1959.

(8) Liao, P. F. In *Surface Enhanced Raman Scattering;* Chang, R. K., Furtak, T. E., Eds.; Plenum Press: New York, 1982.

(9) Hulteen, J. C.; van Duyne, R. P. *J. Vac. Sci. Technol.* **1995**, *13*, 1553.

(10) Preston, C. K.; Moskovits, M. *J. Phys. Chem.* **1988**, *92*, 2957.

(11) Preston, C. K.; Moskovits, M. *J. Phys. Chem.* **1993**, *97*, 8405.

(12) Tierney, M. J.; Martin, C. R. *J. Phys. Chem.* **1989**, *93*, 2878.

(13) Foss, C. A., Jr.; Hornyak, G. L.; Stockert, J. A.; Martin, C. R. *J. Phys. Chem.* **1994**, *98*, 2963.

(14) Yu, Y.; Chang, S.; Lee, C.; Wang, C. R. C. *J. Phys. Chem. B* **1997**, *101*, 6661.

(15) Al-Rawashdeh, N. R.; Sandrock, M. L.; Seugling, C. J.; Foss, C. A., Jr. *J. Phys. Chem. B* **1998**, *102*, 361.

(16) El-Kouedi, M.; Sandrock, M. L.; Seugling, C. J.; Foss, C. A., Jr. *Chem Mater.* **1998**, *10*, 3287.

(17) Van de Hulst, H. C. *Light Scattering by Small Particles*; Dover: New York, 1981.

(18) Bohren, C. F.; Huffman, D. R. *Absorption and Scattering of Light by Small Particles*; Wiley: New York, 1983.

(19) Kreibig, U.; Vollmer, M. *Optical Properties of Metal Clusters,* Springer-Verlag: Berlin, 1995.

(20) Schmitt, J.; Machtle, P.; Eck, D.; Mohwald, H.; Helm, C. A. *Langmuir* **1999**, *15*, 3256.

(21) Furneaux, R. C.; Rigby, W. R.; Davidson, A. P. *Nature* **1989**, *337*, 147.

(22) Shumilova, N. A.; Zutaeva, E. V. In *Encyclopedia of Electrochemistry of the Elements*; Bard, A. J., Ed.; Marcel-Dekker: New York, 1978, 8.

(23) The dimensions of the particles were determined from TEM images. The average length, diameter, spacing distance, and standard deviations were determined from measurements of thirteen to twenty individual structures.

(24) Johnson, P. B.; Christy, R. W. *Phys. Rev. B* **1972**, *6*, 4370.

(25) (a) Meier, M.; Wokaun, A. *Opt. Lett.* **1983**, *8*, 851. (b) Zeman, E. J.; Schatz, G. C. In *Proceedings of the 17th Jerusalem Symposium*; Pullman, B., Jortner, J., Nitzan, A., Gerber, B., Eds.; Reidel: Dordrecht, Holland, 1984; p 413.

(26) For all MLWA and DDA simulations, C_{ext} or Q_{ext} values were calculated at 4 nm intervals from 350 to 800 nm and plotted as continuous curves using Excel software.

(27) Granqvist, C. G.; Hunderi, O. *Phys. Rev. B* **1977**, *16*, 1353.

(28) Purcell, G. M.; Pennypacker, C. R. *Astrophys. J.* **1973**, *186*, 705.

(29) Draine, B. T.; Flatau, P. J. *J. Opt. Soc. Am. A* **1994**, *11*, 1491.

(30) Jensen, T.; Kelly, L.; Lazarides, A.; Schatz, G. C. *J. Cluster Sci.* **1999**, *10*, 295.

(31) In the computation of extinction spectra using the DDSCAT program, the selection of an insufficient number of polarizable elements results in spectral oscillations on the long wavelength side of the plasmon resonance maximum. For each of the spectra in Figure 8, the number of polarizable elements was increased until the oscillations disappeared. We find that the number of polarizable elements required to prevent such oscillations increases as the interparticle spacing decreases.

(32) In the study reported in ref 15, porous aluminum oxide films containing Au rods were impregnated with polyethylene and then exposed to base to dissolve all of the alumina. The Au rods were then mechanically oriented in the plane of the polyethylene film surface. Normal incidence plasmon resonance spectra were obtained at various polarization angles relative to the direction of rod orientation. Significantly, under conditions of parallel polarization, the spectra of the Au rod systems indicated long wavelength resonance bands arising from the particles' long axes. Short wavelength resonances were either absent or present only at very low intensity (consistent with either imperfect orientation of the rod-like particles, or a very small number of spherical Au impurity particles).